Formation of Aminyl Radicals on Electron Attachment to AZT: Abstraction from the Sugar Phosphate Backbone versus One-Electron Oxidation of Guanine

Amitava Adhikary, Deepti Khanduri, Venkata Pottiboyina, Cory T. Rice, and Michael D. Sevilla*

Department of Chemistry, Oakland University, Rochester, Michigan 48309

Received: April 15, 2010; Revised Manuscript Received: June 9, 2010

Employing electron spin resonance (ESR) spectroscopy, we have characterized the radicals formed in 3′-azido-3′-deoxythymidine (3′-AZT) and in its 5′-analog 5′-azido-5′-deoxythymidine (5′-AZT) after electron attachment in γ-irradiated aqueous (H_2O or D_2O) glassy (7.5 M LiCl) systems. ESR spectral studies and theoretical calculations show that the predominant site of electron capture in 3′-AZT and in 5′-AZT is at the azide group and not at the thymine moiety. The azide group in AZT is therefore more electron affinic than the most electron affinic DNA base, thymine. Electron attachment to 3′-AZT and 5′-AZT results in an unstable azide anion radical intermediate ($RN_3\bullet^-$) that is too short-lived to be observed in our work even at 77 K. At 77 K, we observe the neutral aminyl radical (RNH•) after loss of N_2 from $RN_3\bullet^-$ followed by protonation of nitrene anion radical ($RN\bullet^-$) to give RNH•. The expected $RN\bullet^-$ intermediate is not observed as protonation from water is complete at 77 K even under highly basic conditions. Formation of RND• in D_2O solutions confirms water as the source of the NH proton in the RNH•. Our assignments to these radicals are aided by DFT calculations for hyperfine coupling constants that closely match the experimental values. On annealing to higher temperatures (ca. 160−170 K), RNH• undergoes bimolecular hydrogen abstraction reactions from the thymine methyl group and the sugar moiety resulting in the formation of the thymine allyl radical ($UCH_2\bullet$) and two sugar radicals, C3′• and C5′•. RNH• also results in one-electron oxidation of the guanine base in 3′-AZG. This work provides a potential mechanism for the reported radiosensitization effects of AZT.

Introduction

3′-AZT (3′-Azido-3′-deoxythymidine, Scheme 1), an analog of thymidine, also called Zidovudine, is well-known for its antihuman telomerase reverse transcriptase (anti-hTERT) activity.[1] As a result, 3′-AZT is being widely used for treatment of HIV positive patients[1] and it also has been employed as a radiation sensitizer in radiotherapy of tumors for HIV positive patients.[2]

Recently, 3′-AZT has been shown to act as a radiosensitizer in irradiated tumor cells; for example, the studies employing HeLa cells exposed to different doses of γ-radiation in the presence of an aqueous solution (0.1 μM) of 3′-AZT show a direct correlation between cell survival and micronuclei-induction.[3] Also, in irradiated human colon cancer cells,[4] in irradiated human larynx squamous carcinoma cells,[5] and in irradiated human malignant glioma cells,[6] 3′-AZT has been shown to be a significant radiosensitizer. Furthermore, it has been reported that 3′-AZT substantially enhances γ-irradiation killing of EBV (Epstein−Barr virus)-transformed lymphoblastoid cells in vitro.[7]

The chemical pathways involved in the radiosensitization provided by 3′-AZT are still unknown. However, from the literature, we have found clues regarding likely chemical pathways based on studies carried out on other azides. For example, phenyl azide (PhN_3) upon gas phase electron attachment leads to the production of the phenylnitrene anion radical ($PhN\bullet^-$) via loss of nitrogen.[8] The nitrene anion radicals have been found to be highly reactive and have a very high proton affinity (PA).[8,9] For example, the proton affinity of $PhN\bullet^-$ was found to be 372 ± 2 kcal/mol.[8] These nitrene anion radicals protonate rapidly to form the aminyl radical (PhNH•) with proton donors.[8,9] Zhu and Schuster[10] observed that absorption of light by the biphenyl chromophore in the *N*-biphenylylpiperidinyl-substituted benzoyl azides (BPA) in aqueous solutions led to the formation the amine in the site of the azide. From these results, they had proposed that the azide anion radical ($RN_3\bullet^-$) produced via long-range intramolecular electron transfer underwent a rapid loss of N_2 to form the nitrene anion radical ($RN\bullet^-$);[10] $RN\bullet^-$ likely formed the RNH• species via protonation, and finally, the RNH• species led to the amine (RNH_2) product via hydrogen abstraction.[10] Investigations of light-catalyzed reduction of aromatic azides to amines employing CdS and CdSe nanoparticles had also suggested that reduction of aromatic azides to amines proceeded via formation of a similar nitrene anion radical, $RN\bullet^-$ and the corresponding protonated species RNH•, led to formation of amine by hydrogen abstraction from the solvent.[11]

Thus the previous literature suggests the following mechanism for the formation of amines from organic azides initiated by one-electron reduction

Azide anion radical formation

$$RN_3 + e^- \rightarrow RN_3\bullet^- \quad (1)$$

* To whom correspondence should be addressed. E-mail: sevilla@oakland.edu. Phone: 001 248 370 2328. Fax: 001 248 370 2321.

10.1021/jp103403p
Published on Web 06/24/2010

SCHEME 1: Structural Formula of 3′-Azido-3′-deoxythymidine (3′-AZT), 5′-Azido-5′-deoxythymidine (5′-AZT), and 3′-Azido-2′,3′-dideoxyguanosine (3′-AZG)

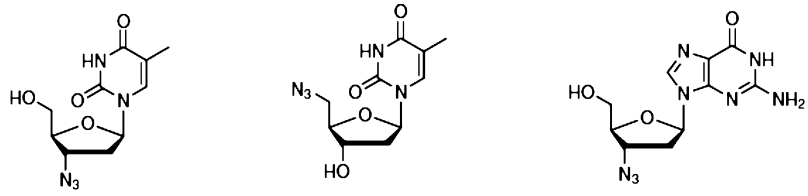

3'-azido-3'-deoxythymidine 5'-azido-5'-deoxythymidine 3'-azido-2',3'-dideoxyguanosine

Nitrene anion radical formation

$$RN_3\bullet^- \rightarrow RN\bullet^- + N_2 \quad (2)$$

Aminyl radical formation

$$RN\bullet^- + H_2O \rightarrow RNH\bullet \quad (3)$$

Amine formation by H-atom abstraction

$$RNH\bullet + R'-H \rightarrow RNH_2 + R'\bullet \quad (4)$$

Amine formation by one-electron reduction

$$RNH\bullet + e^- + H_2O \rightarrow RNH_2 + OH^- \quad (5)$$

To date, no ESR observation of the proposed radical intermediates shown in reactions 1 to 5 has been reported for AZT or any other molecules containing azide.

In this report, the radicals formed after one-electron attachment at 77 K to 3′-AZT, its 5′- analog, 5′-azido-5′-deoxythymidine (5′-AZT), and 3′-azido-2′,3′-dideoxyguanosine (3′-AZG) (Scheme 1) have been characterized and identified by ESR spectroscopy. Our work shows that one-electron addition to the azide group of AZT results in a highly reactive aminyl radical (RNH•). In accordance with the highly reactive nature of the neutral aminyl radicals,[12] RNH• has been found to be a potent H-atom abstracting agent that leads to base damage and sugar radicals that are known DNA-strand break precursor radicals.[13] It is well-known that aqueous electrons do not produce DNA strand breaks.[13] Thus, the conversion of "near harmless" aqueous electrons to the highly reactive RNH• in 3′-AZT suggests that 3′-AZT and its analogs could be used as effective radiosensitizers in low-oxygen (bioreductive) environments.[14]

Materials and Methods

1. Compounds. 3′-Azido-3′-deoxythymidine (3′-AZT), 5′-azido-5′-deoxythymidine (5′-AZT), and 3′-azido-2′,3′-dideoxyguanosine (3′-AZG) were purchased from Berry & Associates, Inc. (Dexter, MI). Lithium chloride (99% anhydrous, SigmaUltra) was procured from Sigma Chemical Company (St. Louis, MO). Deuterium oxide (D_2O, 99.9 atom % D) was purchased from Aldrich Chemical Co., Inc. (Milwaukee, WI). All the compounds were used without any further purification.

2. Preparation of Solutions of 3′-AZT, 5′-AZT, and 3′-AZG. Following the previous works regarding electron attachment reactions and transfer in DNA from our laboratory,[15−17] homogeneous solutions of 3′-AZT, 5′-AZT, and 3′-AZG were prepared by dissolving ca. 0.5 mg of each compound in 1 mL of 7.5 M LiCl in H_2O or in D_2O.

3. Preparation of Glassy Sample and Their Storage. Following our previous work,[18−21] the transparent glassy samples of 3′-AZT, 5′-AZT, and 3′-AZG were prepared in 4 mm Suprasil quartz tubes (cat. no 734-PQ-8, WILMAD Glass co., Inc., Buena, NJ). These glassy samples were stored in the dark at 77 K.

4. pD Adjustments. Following our work with nucleosides and oligomers,[18−21] pD of homogeneous solutions of 3′-AZT were adjusted to ca. 12 by adding incremental amounts of μL volumes of 1 M NaOH under ice-cooled condition.

5. γ-Irradiation and Storage of Irradiated Samples. As per our earlier work,[18−21] these glassy samples were γ-irradiated with the aid of a 109-GR 9 irradiator containing a shielded ^{60}Co source with an absorbed dose of 525−700 Gy (45 min to 1 h) at 77 K and were stored at 77 K in Teflon containers in the dark before recording the ESR spectra of these irradiated samples at 77 K in the dark.

Owing to the irradiation of the 7.5 M LiCl glass (H_2O or D_2O) with only 0.5 mg sample per ml, nearly all of the initial ionization takes place in the solution thereby creating matrix electrons and holes. The electrons are scavenged by the solute (for example, 3′-AZT) and the holes remain in the glass as $Cl_2\bullet^-$.

6. Photoexcitation. By employing a photoflood lamp (250 W), the γ-irradiated glassy samples of 3′-AZT and 5′-AZT were photoexcited in the suprasil quartz dewar (cat. no WG-816(-Q), WILMAD Glass co., Inc. Buena, NJ) at 77 K for 15 min, which photoejects the electron from the thymine anion radical. The electron subsequently reacts with the azide group and forms the aminyl radical (R−NH•). After photoexcitation, these samples were stored at 77 K in the dark before carrying out the ESR spectral studies of these samples.

7. Thermal Annealing and Storage of These Samples. Following our previous works,[18−21] the γ-irradiated and subsequently photoexcited samples were annealed in the dark in a variable temperature assembly (Air Products) in the temperature range 140−175 K employing cooled nitrogen gas. These transparent glassy samples are not crystalline solids. Rather, they are supercooled homogeneous solutions. These supercooled solutions soften on warming via progressive thermal annealing at higher temperatures; this softening facilitates molecular migration in these solutions thereby allowing solution phase chemistry. After annealing, these samples were immediately immersed in liquid nitrogen (77 K) for ESR analysis.

8. Electron Spin Resonance. The ESR spectra of samples were recorded in the suprasil quartz dewar (cat. no WG-850(-Q), WILMAD Glass co., Inc., Buena, NJ) at 77 K and at 45 dB (6.3 μW) using a Varian Century Series ESR spectrometer operating at 9.2 GHz with an E-4531 dual cavity, 9 in. magnet and with a 200 mW klystron. For field calibration, Fremy's salt (g (center of the spectrum) = 2.0056, A_N = 13.09 G) has been employed following our earlier works.[18−21]

9. Analyses of ESR Spectra. As per our earlier works,[18−21] each ESR spectrum was stored in a 1000 point array along with field calibration marks from the three ESR lines of the Fremy's salt. The fractional contribution of a radical species in an experimentally obtained ESR spectrum has been estimated by

SCHEME 2: B3LYP/6-31G* Optimized Structure of the Azide Anion Radical (T(C3′)-N_3•$^-$) and the Aminyl Radical (T(C3′)-NH•) of 3′-AZT and the Aminyl Radical T(C5′)-NH• of 5′-AZ[a]

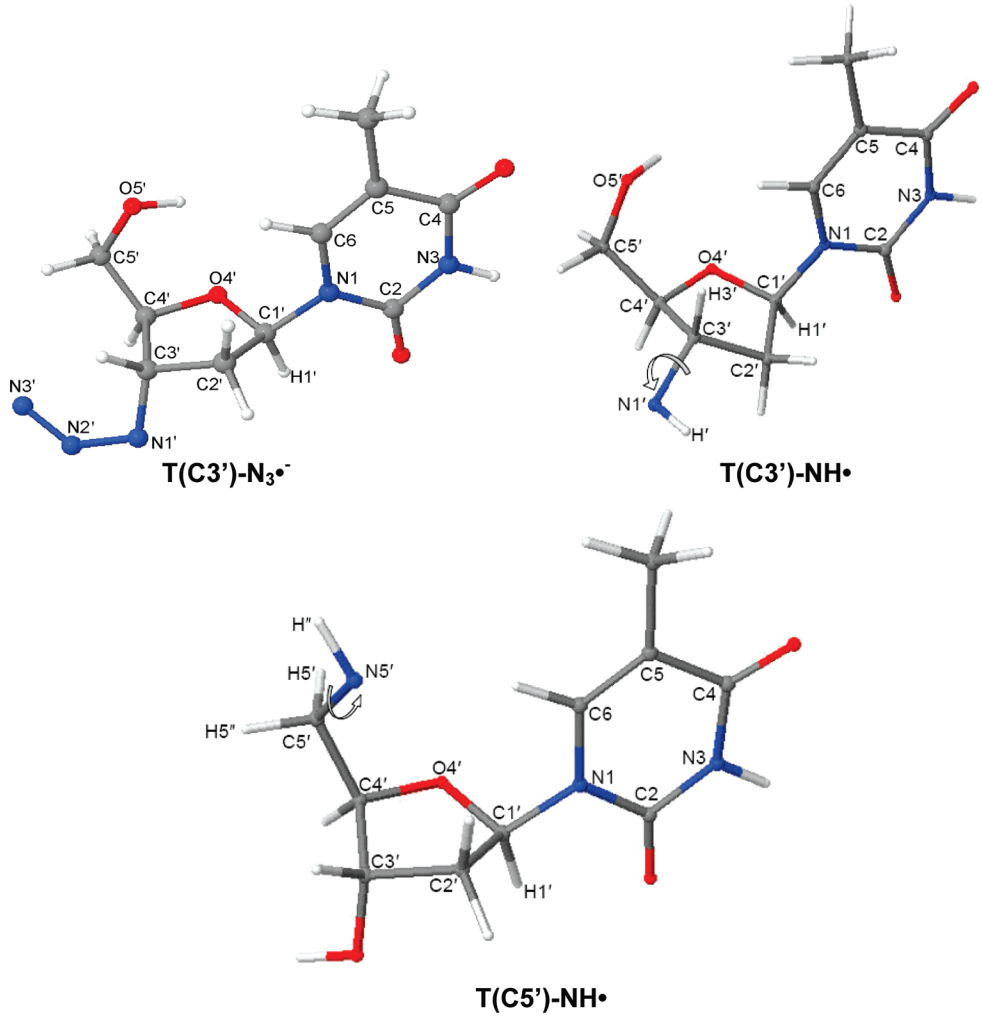

[a] The atom numbering scheme shown in this scheme is used in this work. In T(C3′)-NH•, the N1′−H' bond can rotate around the C3′−N1′ bond (as shown by the arrow). Similarly, in the corresponding aminyl radical (T(C5′)-NH•) of 5′-AZT, rotation of the N5′−H″ bond is possible around the C5′−N5′ bond (as indicated by the arrow).

fitting the benchmark spectrum of that particular radical to the experimentally obtained ESR spectrum of interest using least-squares analyses by employing programs (ESRADSUB, ESRPLAY) developed in our laboratory.[18−21] The error limit of these above-mentioned analyses has been estimated as ±10% with good quality signals.[18] We have subtracted a small singlet "spike" from irradiated quartz at $g = 2.0006$ from the recorded spectra for our analyses.

10. Theoretical Calculations. The geometries of the azide anion radical, nitrene anion radical, and aminyl radical shown in reactions 1 to 5 involving 3′-AZT and 5′-AZT were fully optimized by employing the B3LYP functional and the 6-31G* basis set. The B3LYP functional is a Becke's three parameter exchange functional (B3)[22] with Lee, Yang, and Parr's correlational functional (LYP).[23] We have performed all calculations by employing the Gaussian 03 suites of programs.[24] The applicability of the B3LYP functional for the DFT calculations of HFCC values of radical species is well established in the literature.[25−27] The structures were drawn using JMOL molecular modeling program.[28] The atom numbering scheme of AZT used in this work also indicates the rotation of (i) the N1′−H′ bond around the C3′−N1′ bond in T(C3′)-NH•, and (ii) the N5′−H″ bond around the C5′−N5′ bond in T(C5′)-NH• are shown in Scheme 2.

Results and Discussion

1. Experimental Studies. ***A. Reactions Due to Electron Attachment in 3′-AZT.*** *A.1. Studies in D_2O.*

A.1.1. The Experimental Spectra. Figure 1A shows the radicals formed after γ-irradiation of a 7.5 M LiCl (D_2O) glass containing 3′-AZT (Figure 1A). Irradiation of 7.5 M LiCl glasses produces Cl_2•$^-$ and a small amount of deuterium atom (D•) in addition to electrons. The isolated spectrum of Cl_2•$^-$ has been superimposed on the experimentally recorded spectrum (black) for comparison. In Figure 2A−C, we show the spectra from those already presented in Figure 1A−C after subtraction of the Cl_2•$^-$ and D•, which isolates the radicals formed via the one-electron reduction process.

The central doublet in Figures 1A and 2A is assigned to the thymine anion radical (T•$^-$) as it is identical to the spectrum of T•$^-$ reported in the literature.[29] Furthermore, the black-colored spectrum shown in Figure 1A (and also in Figure 2A) has the line components due to the neutral aminyl radical (T(C3′)-ND•) (see Figure 2A and its discussion below).

Photoejection of the electron from the T•$^-$ via visible photoexcitation at 77 K results in the spectra shown in Figure 1B and in Figure 2B (after subtraction of Cl_2•$^-$). Because of the absence of the central doublet owing to T•$^-$ in the black-

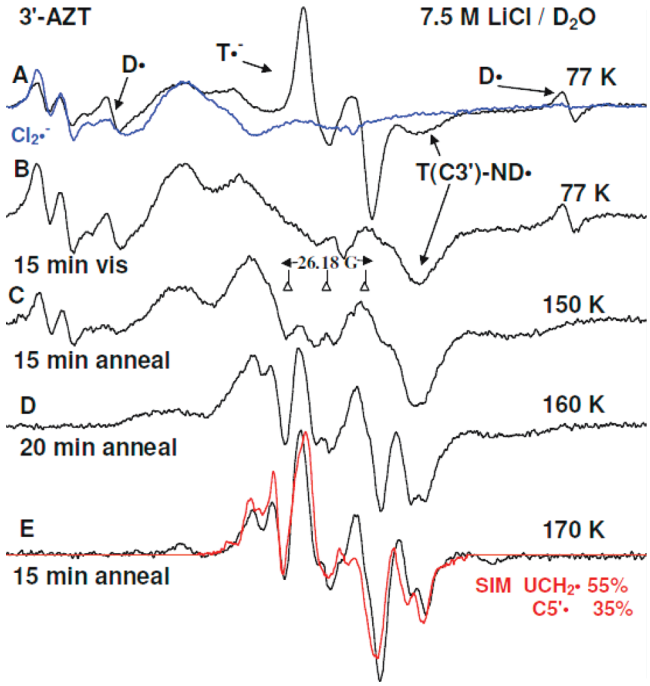

Figure 1. First derivative ESR spectrum (A) (black) for 3′-AZT after one-electron addition at 77 K at the native pD (ca. 5) of the homogeneous glassy solution of 7.5 M LiCl in D_2O. For comparison, the ESR spectrum of $Cl_2^{\bullet-}$ in D_2O (7.5 M LiCl) (blue) has been superimposed on it. (B) ESR spectrum (black) after visible illumination of the sample by using a photoflood lamp at 77 K for 15 min to remove the thymine anion radical by photoejection of the excess electron. ESR spectrum (black) of this sample after subsequent annealing in the dark at (C) 150 K for 15 min, (D) 160 K for 20 min, and (E) 170 K for 15 min. The spectrum shown in red in panel E is a simulated spectrum employing ca. 55% of the UCH_2• spectrum,[30] and 35% C5′• spectrum (doublet ca. 19 G).[21a] The remaining 10% is accounted for by another radical (probably, at the C3′ site which is not included in the simulation). This is evidenced by the outermost line components in low intensity. All ESR spectra shown in panels A−E were recorded at 77 K. The three reference markers in this figure and in subsequent figures are Fremy's salt resonances with central marker is at $g = 2.0056$ and each of three markers is separated from one another by 13.09 G.

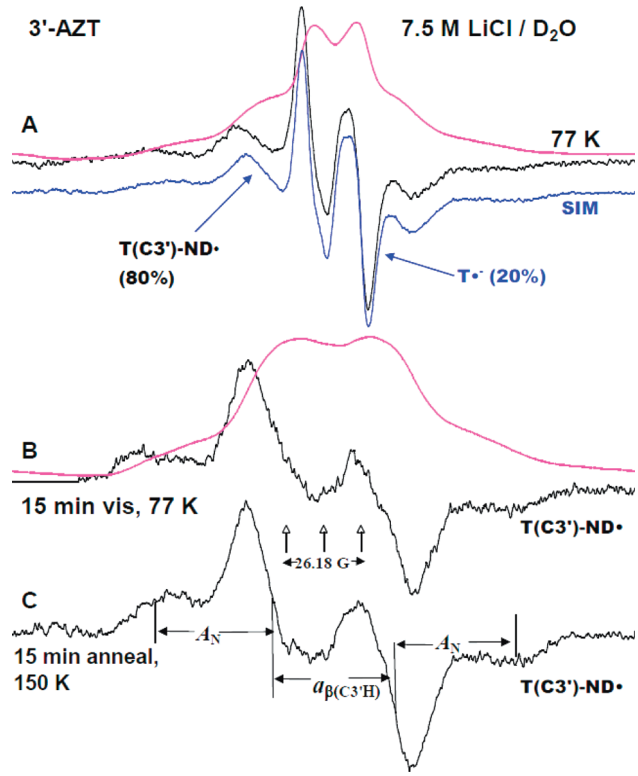

Figure 2. (A) ESR spectrum (black) from Figure 1A after subtraction of the appropriate amounts of the D• and $Cl_2^{\bullet-}$ spectra. The spectrum shown in blue is a simulated spectrum employing ca. 80% of the spectrum (black) assigned to the aminyl radical (T(C3′)-ND•) shown in panel B, and 20% of the $T^{\bullet-}$ spectrum.[29] (B) ESR spectrum (black) obtained by subtracting the appropriate amount of the D• and $Cl_2^{\bullet-}$ spectra from the spectrum in Figure 1B and is assigned to T(C3′)-ND•. The spectra in pink in A and B are the single integration of the black spectra and show the dominance of the T(C3′)-ND• species in panel A. (C) The ESR spectrum (black) found after subtracting 35% of the black-colored spectrum in Figure 1E along with subtraction of appropriate amount of $Cl_2^{\bullet-}$ spectrum from the spectrum in Figure 1C. This spectrum is nearly identical of that shown in panel B and is also assigned to T(C3′)-ND•. The extent of β-hyperfine coupling by H3′-atom and the anisotropic nitrogen hyperfine coupling, $A_{||}$ in T(C3′)-ND•, are indicated by stick diagrams. They indicate that the central doublet in both (B) and (C) arises from the H3′ β-hyperfine coupling and the line components of the anisotropic nitrogen hyperfine coupling (see text and Table 1).

colored spectrum in Figure 1B (or in Figure 2B), we conclude that the electron is completely photoejected from T and reacts to produce additional T(C3′)-ND•. An analysis of the spectrum in Figure 2A, taking ca. 80% of the spectrum (black) in Figure 2B assigned to the aminyl radical (T(C3′)-ND•) and 20% of $T^{\bullet-}$[29], results in the simulation shown in blue under the spectrum (black) shown in Figure 2A. The simulated spectrum (blue) matches the spectrum (black) very well. Added support for this analysis comes from the pink-colored spectra shown in Figure 2A,B. These result from the single integration of the first derivative ESR spectra in black and the area under these curves is proportional to the radical intensity. A comparison shows that the spectrum of T(C3′)-ND• (black, Figure 2B) accounts for the predominant share of the radical intensity of T(C3′)-ND• in Figure 2A in agreement with the analysis described above.

These results establish the following:

(i) The preponderance (ca. 80%) of the aminyl radical (T(C3′)-ND•) over that of the $T^{\bullet-}$ (ca. 20%) shows that the site of electron capture in 3′-AZT is predominantly at the azide group and not at the thymine moiety. This suggests that the azide group in 3′-AZT is more electron affinic than thymine, the most electron affinic DNA base.

(ii) Electron attachment to 3′-AZT at 77 K results in only the neutral aminyl radical (T(C3′)-ND•) not the azide anion radical (T(C3′)-$N_3^{\bullet-}$) or the nitrene anion radical (T(C3′)-$N^{\bullet-}$). This indicates that the azide anion radical (T(C3′)-$N_3^{\bullet-}$) is unstable and loses N_2 immediately to form the corresponding nitrene anion radical (T(C3′)-$N^{\bullet-}$), which undergoes protonation to form the aminyl radical, (T(C3′)-ND•). Thus, reactions 1−3 are complete even at 77 K.

Subsequent annealing of this sample at 150 K for 15 min leads to the spectrum in Figure 1C. Comparison of this spectrum with that shown in Figure 1B shows that there is almost no loss of intensity upon annealing from 77 K to ca. 150 K. Further, spectrum in Figure 1C shows that at this temperature the $Cl_2^{\bullet-}$ produced initially has largely diminished and the line components due to (T(C3′)-ND•) remain (see comparison between Figures 2B and 2C).

In Figure 2C, we present the spectrum found after subtracting 35% of black-colored spectrum in Figure 1E along with appropriate amount of $Cl_2^{\bullet-}$ spectrum from the spectrum 1C. The total hyperfine splitting of ca. 116 G, the individual hyperfine couplings, and the g-values of spectrum (black) shown in Figure 2C are nearly identical to those found for spectrum

TABLE 1: Hyperfine Couplings and *g*-Values for the Neutral Aminyl Radicals Found in 3′-AZT and in 5′-AZT at 77 K

		hyperfine couplings (G)				
radical		exp		theory		g-value (exp)
3′-AZT T(C3′)-NH•	H3′(β-proton, isotropic)	41		40		$g_{\|\|} = 2.0020$, $g_{\perp} = 2.0043$
	N1′-H′(α-proton)	(*,*, −28)[a,b]		(−39.5, 0.4,−26.4)		
	N1′-coupling	(0, 0, 37.5)		(0, 0, 41.4)		
		sum[c]	angle	A(H5′,H5″)	sum	
5′-AZT T(C5′)-NH•	β-protons, (H5′, H5″)	91 [d]	40°	(30,57)	87 G	$g_{\|\|} = 2.0020$, $g_{\perp} = 2.0043$
			60°	(50,42)	92 G	
			80°	(62,23)	85 G	
	N5′-H″ (α-proton)	(*, *, −30)[a,b]		(−39.8, 0.4, −26.7)		
	N1′-coupling	(0, 0, 43)		(0, 0, 41.8) G		

[a] From the width of the experimentally recorded spectra (see Figures 3 and 5), only $A_{||}$ (i.e., the A_{zz}) component could be determined. [b] The simulation of the experimental spectrum for T(C3′)-NH• (see Figures 3 and Supporting Information S1) was carried out by employing the DFT calculated A_{xx} and A_{yy} values along with the experimentally obtained A_{zz} value i.e., (−39.5, 0.4, −28) G. [c] Angle = H5″−C5′−N5′−H″ dihedral angle; A(H5′,H5″) are the isotropic hyperfine couplings of H5′, H5″ at those dihedral angles; Sum = the sum of these isotropic hyperfine couplings. [d] See Figure 5.

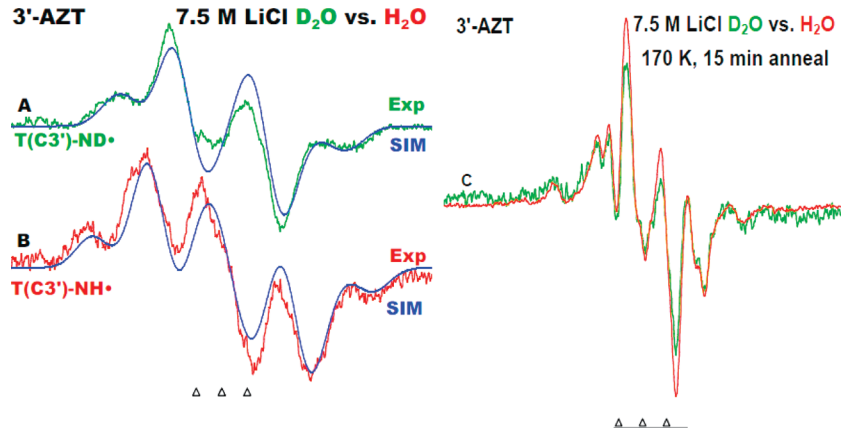

Figure 3. First derivative ESR spectrum of the aminyl radical formed via one-electron attachment by γ-irradiation of 3′-AZT (A) (T(C3′)-ND•) (green color) in 7.5 M LiCl (D_2O), (B) (T(C3′)-NH•) (red color) in 7.5 M LiCl (H_2O). The green color spectrum in (A) is the same one shown in Figure 2C. The simulated spectra (blue) (for simulation ESR parameters, see Supporting Information S1) are superimposed on the top of the experimentally recorded spectrum. Comparison of these two spectra clearly shows the $A_{||}$ (i.e., the A_{zz}) component ca. 28 G due to the α-N−H proton of the aminyl radical in H_2O (T(C3′)-NH•) (red color) is lost in the D_2O glasses (green color). (C) Further annealing of this sample in 7.5 M LiCl (H_2O) in the dark at 170 K for 15 min leads to the spectrum (green) recorded at 77 K. For comparison, the ESR spectrum obtained via annealing of T(C3′)-ND• at 170 K for 15 min in the dark in D_2O (7.5 M LiCl) (red) from Figure 2D, has been superimposed on it.

shown in Figure 2B and is also assigned to T(C3′)-ND•. The central doublet (ca. 41 G) found in Figure 2B,C arises from an isotropic β-proton coupling assigned to the 3′ proton. The wings of this spectrum show the line components of the anisotropic nitrogen hyperfine coupling, $A_{||}$, of ca. 37.5 G, $A_{\perp} = 0$ due to a single N-atom assigned to the aminyl nitrogen with $g_{||} = 2.0020$ and $g_{\perp} = 2.0043$. The hyperfine coupling of the aminyl N-atom and the β-proton coupling from H3′ are illustrated by stick diagrams (see Figure 2C). The stick diagram shows the major splittings roughly; however, a full anisotropic simulation given in Figure 3A provides strong evidence for our analysis.

Further annealing of this sample at 160 K for 20 min and subsequently at 170 K for 15 min lead to the spectra (black) shown in Figure 1D,E respectively. Each spectrum was recorded at 77 K. Comparison of the spectrum in Figure 1C (annealing at 150 K) with that of Figure 1D (annealing at 160 K) shows the decrease of the line components due to T(C3′)-ND• along with the concomitant development of the line components at the center due to other radicals (see below). In the spectrum shown in Figure 1E, T(C3′)-ND• has fully reacted by bimolecular hydrogen abstraction from the methyl group and sugar of a nearby 3′-AZT molecule resulting in the thymine allyl radical (UCH_2•),[30] and sugar radical, C5′• (doublet ca. 19 G).[21a] On this basis, we have simulated a spectrum (red) by adding ca. 55% of the UCH_2•, and 35% C5′• spectrum. This simulated spectrum matches the experimentally recorded spectrum (black) in Figure 1E well except for the outermost weak lines. These outermost weak line components (outermost lines at ca. 94 G) may be due to C3′•. These small components (ca. 10%) do not contribute significantly to the spectral intensity and are not included in the simulation. We, therefore, find evidence for H-abstraction by T(C3′)-ND• from the thymine methyl group as well as possibly two sugar sites (C5′, C3′).

A.2. Studies in D_2O versus H_2O. Identical ESR spectral studies of electron attachment to 3′-AZT in H_2O glasses (7.5 M LiCl/H_2O) were also performed and are compared with the results found in D_2O glasses (7.5 M LiCl/D_2O) and are shown in Figure 3 below.

Figure 3A presents the first derivative ESR spectrum of the aminyl radical (T(C3′)-ND•) (green color) shown in Figure 2C.

The first derivative ESR spectrum of the aminyl radical (T(C3′)-NH•) (red color) obtained under identical conditions (annealed at 150 K in the dark for 15 min and recorded at 77 K) from 3′-AZT in H_2O (7.5 M LiCl) is shown in Figure 3B.

Comparison of widths of these two spectra clearly shows that an additional 28 G proton hyperfine coupling in the aminyl radical in H_2O (T(C3′)-NH•) (red color) is present in the H_2O glasses and is missing in the D_2O glasses (green color). These

results show that the source of the proton in the formation of the aminyl radical (T(C3′)-NH•) via protonation (reaction 3 of the nitrene anion radical (T(C3′)-N•$^-$)) is the solvent (H_2O). This additional hyperfine coupling of 28 G is the $A_{||}$ (i.e., the A_{zz}) component of the N−H (α-H) coupling that contributes to the outer line components and this component adds to the $A_{||}$ component of the anisotropic hyperfine coupling of the N-atom of T(C3′)-NH• (see Table 1). Thus, from the experimentally recorded spectrum (red) of T(C3′)-NH• (Figure 3B), only the $A_{||}$ (i.e., the A_{zz}) component of the N−H (α-H) hyperfine coupling could be determined.

The spectrum of T(C3′)-ND• in Figure 3A and that of the T(C3′)-NH• in Figure 3B have been simulated (blue color) by employing the DFT calculated $A_\perp$ along with the experimentally obtained $A_{||}$ values for the N−H hyperfine coupling, that is, (−39.5, 0.4, −28) G for T(C3′)-NH• (see Table 1 for couplings employed) and the simulated spectra match quite well with that of the experimentally observed spectra (more detailed ESR parameters employed such as linewidths and lineshapes for simulations of the experimentally found spectra in Figure 3 are mentioned in Supporting Information S1).

The hyperfine couplings of T(C3′)-NH• have been theoretically calculated (DFT/B3LYP/6-31G*) (see Section 2.2 and Table 1). The theoretically calculated values of the hyperfine couplings match very well (see Table 1) with experimental values.

Further annealing of this sample at 170 K for 15 min leads to the spectrum (green) recorded at 77 K and is shown in Figure 3C. For comparison, the ESR spectrum obtained via annealing of T(C3′)-ND• at 170 K for 15 min in the dark in D_2O (7.5 M LiCl) (red) from Figure 1E has been superimposed on it. The very close match of these two spectra clearly establish that (i) the radical cohort (UCH_2•, C3′•, C5′•) formed in 3′-AZT due to bimolecular hydrogen abstraction by the aminyl radical (T(C3′)-NH•) in homogeneous H_2O glasses (7.5 M LiCl/H_2O) has very similar population of radicals to that for the corresponding reaction by the aminyl radical (T(C3′)-ND•) in homogeneous D_2O glasses (7.5 M LiCl/D_2O), and (ii) as expected, there is no observable solvent isotope effect (H_2O vs D_2O) for the bimolecular hydrogen abstraction from 3′-AZT by the aminyl radical (T(C3′)-ND• or (T(C3′)-NH•).

A.3. Studies in D_2O at High pH. Electron attachment reactions to 3-AZT were carried out in 7.5 M LiCl in D_2O at higher pD (ca. 12) to observe the ESR spectral signatures of the parent nitrene radical (T(C3′)-N•$^-$) as shown in reaction 3. Contrary to our expectation, the ESR spectrum of the neutral aminyl radical (T(C3′)-ND•) was observed in 3′-AZT at the pD (ca. 12) of the 7.5 M LiCl/D_2O (see Supporting Information Figure S2). Thus, even at pD ca. 12, the protonation of the nitrene anion radical (T(C3′)-N•$^-$) leads to the complete formation of the neutral aminyl radical (T(C3′)-ND•) (reaction 3) from the solvent (D_2O) at 77 K. These results are in accord with the known high proton affinity of the parent nitrene radical which has been reported for phenyl nitrine anion radical, PhN•$^-$ to be 372 ± 2 kcal/mol.[8]

B. Reactions Due to Electron Attachment in 5′-AZT. The ESR spectra of the radicals formed in 5′-AZT (see Scheme 1) via electron attachment, followed by the photodetachment of the electron from the incipient thymine anion radicals at 77 K and by annealing at higher temperatures are shown in the Figure 4.

Following Figure 2, all the black-colored spectra shown in Figure 4A−C are found after subtracting the Cl_2•$^-$ and/or D• spectra. Supporting Information Figure S3 shows the original

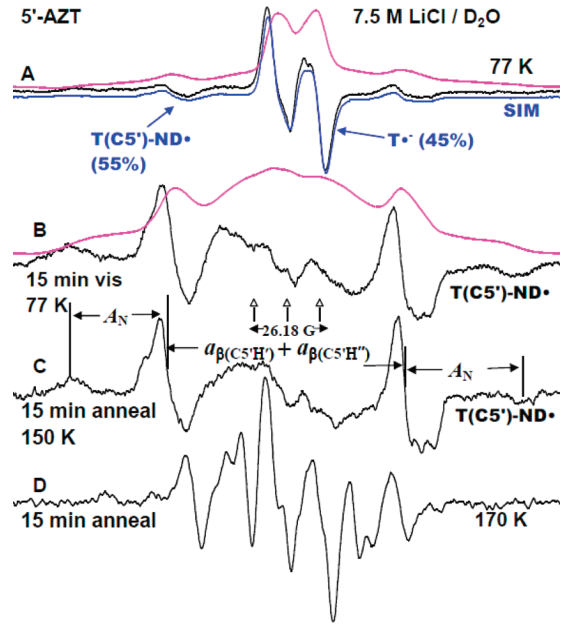

Figure 4. All the black-colored spectra shown in panels A−C are found after subtracting spectra of Cl_2•$^-$ and/or D• from the experimental spectra. (A) ESR spectrum (black) for 5′-AZT after one-electron addition at 77 K in 7.5 M LiCl in D_2O. The spectrum shown in blue is the simulated spectrum by employing ca. 55% (T(C5′)-ND•) shown in panel B, and 45% of reported spectrum[29] of T•$^-$. (B) ESR spectrum (black) recorded at 77 K after visible illumination of the sample by using a photoflood lamp at 77 K for 15 min to remove the T•$^-$ by photoejection of the excess electron. The central doublet (ca. 91 G) found in this spectrum is due to the sum of two isotropic β-proton couplings and, the wings of this spectrum show the line components of the anisotropic nitrogen hyperfine coupling (see text and Table 1). This spectrum shown is assigned to T(C5′)-ND•. The spectra in pink in A and B are the single integration of the experimentally recorded first derivative ESR spectra (black). (C) ESR spectrum of this sample after subsequent annealing of this sample in the dark at 150 K for 15 min. This spectrum shows only minor coupling changes from that shown in panel B and is assigned to T(C5′)-ND•. The stick diagram shows the β-proton couplings and parallel component of nitrogen coupling. (D) After subsequent annealing in the dark at 170 K for 15 min. This spectrum is assigned to C3′ and UCH2 radicals. All ESR spectra in panels A−D were recorded at 77 K.

spectra of all the radicals formed by γ-irradiation of 5′-AZT in a 7.5 M LiCl glass in D_2O and subsequent annealing before subtraction.

The ESR spectrum of the radicals produced via electron attachment in 5′-AZT is shown in Figure 4A. Similar to the results found for the spectrum for 3′-AZT shown in Figure 2A, spectrum in Figure 4A also consists of thymine anion radical (T•$^-$) and the neutral aminyl radical (T-(C5′)-ND•). The spectrum shown in Figure 4B is assigned to the neutral aminyl radical (T-(C5′)-ND•) (vide infra), after the ejection of the electron from the thymine moiety via photoexcitation at 77 K.

The experimentally obtained spectrum (black) in Figure 4A was simulated by taking ca. 55% of the spectrum (black) assigned to the neutral aminyl radical (T(C5′)-ND•) shown in Figure 4B and the remaining 45% of reported spectrum[29] of T•$^-$. This simulated (blue) ESR spectrum is presented just under the experimentally recorded spectrum (black) in Figure 4A. The close match between simulated and experimental spectra in Figure 4A allows us to conclude that the radical cohort found in the experimentally recorded spectrum (black) consists of ca. 55% of aminyl radical (T(C5′)-ND•) and of ca. 45% of T•$^-$.

Moreover, similar to the analyses of spectrum in Figure 2A, the detection of only the neutral aminyl radical (T(C5′)-ND•)

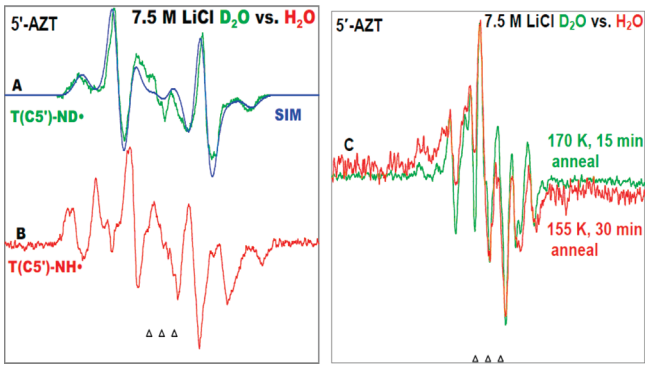

Figure 5. First derivative ESR spectrum of the aminyl radical formed via one-electron attachment by γ-irradiation of 5′-AZT (A) (T(C5′)-ND•) (green color) in 7.5 M LiCl (D_2O), (B) (T(C5′)-NH•) (red color) in 7.5 M LiCl (H_2O). The green color spectrum in panel A is the same one shown in panel B. The simulated spectrum (blue) (for ESR simulation parameters, see Supporting Information S4) is superimposed. Comparison of spectra in D_2O and H_2O clearly shows that the $A_{||}$ (i.e., the A_{zz}) component ca. 30 G due to the α-N−H proton of the aminyl radical is found in H_2O (T(C5′)-NH•) (red color) but not in D_2O glasses (green color). (C) Further annealing of this sample in 7.5 M LiCl (H_2O) in the dark at 155 K for 30 min leads to the spectrum (red) recorded at 77 K. For comparison, the ESR spectrum obtained via annealing of T(C5′)-ND• at 170 K for 15 min in the dark in D_2O (7.5 M LiCl) (green color) from Figure 4D, has been superimposed on it.

and not the azide anion radical (T(C5′)-N_3•$^-$) or the nitrene anion radical (T(C5′)-N•$^-$) after electron attachment in 5′-AZT in the experimentally recorded spectrum (black color) shown in the Figure 4A at 77 K shows that the azide anion radical (T(C5′)-N_3•$^-$) formation represented in reaction 1, the nitrene anion radical (T(C5′)-N•$^-$) via loss of N_2 shown in reaction 2, and the protonation of the nitrene radical leading to the formation of the aminyl radical, (T(C5′)-ND•) (reaction 3) are all complete at 77 K .

In Figure 4B, the first derivative ESR spectrum (black) recorded at 77 K after visible illumination of this sample at 77 K for 15 min to photoeject the electron from thymine is presented. The total hyperfine splitting of this spectrum (black) is ca. 177 G. The wings of this spectrum shows the line components of the anisotropic nitrogen hyperfine coupling, $A_{||}$, of ca. 43 G, $A_{\perp} = 0$ due to a single N-atom with $g_{||} = 2.0020$ and $g_{\perp} = 2.0043$. Moreover, this spectrum also shows a prominent doublet like feature with a total width of ca. 91 G. In Figure 4B, the single integration of the recorded first derivative ESR spectrum (black) is shown by the pink-colored spectrum that is superimposed on the top of the experimentally obtained first derivative spectrum (black) for comparison. The area under the pink spectrum in Figure 4B shows that the doublet-like feature (ca. 91 G) is a sum of two β proton hyperfine couplings (ca. 60 and ca. 31 G). Therefore, the black-colored spectrum shown in Figure 4B is assigned to T(C5′)-ND•, where the radical site is on the one N-atom from the azide group and the two β-proton hyperfine couplings are due to the two H-atoms attached to the C5′-carbon atom in the sugar moiety. A full anisotropic simulation of this spectrum in provided in Figure 5A using the parameters above (see Supporting Information S4 for complete details. The spectrum of T(C5′)-ND• shown in Figure 4B has been used as a benchmark spectrum for analyses of the spectrum (black) shown in Figure 4A (vide supra).

A comparison of the experimentally recorded (black) spectrum in Figure 4B with that (black) of Figure 4A shows visible excitation at 77 K for 15 min photoejects the electron completely from T•$^-$. The ejected electron subsequently reacts with the azide group in 5′-AZT thereby increasing the amount of neutral aminyl radical (T(C5′)-ND•).

In Figure 4C, the spectrum (black) recorded at 77 K after subsequent annealing of this sample in the dark at 150 K for 15 min is shown. No new radicals are found and the total hyperfine splitting of T(C5′)-ND• increases slightly to (ca. 178 G). The parameters of the anisotropic hyperfine coupling due to a single N-atom ($A_{||}$, of ca. 42 G, $A_{\perp} = 0$ with $g_{||} = 2.0020$ and $g_{\perp} = 2.0043$) remains unchanged but the sum of the two β-H hyperfine couplings increases to ca. 94 G as shown from the apparent doublet (black) in Figure 4C. Therefore, this spectrum is also assigned to the neutral aminyl radical (T(C5′)-ND•). The hyperfine coupling of the N-atom and the two β-H couplings in T(C5′)-ND• due to H5′ and H5″ atoms are illustrated by stick diagrams (see Figure 4C).

In Figure 4D, the spectrum (black) recorded at 77 K after further annealing of this sample in the dark at 170 K for 15 min is shown. Unlike Figure 2D for 3′-AZT, the spectrum in Figure 4D appears to be predominantly from one radical having a 1:1:2:2:1:1 pattern expected from three β-proton couplings. The three β-protons and the total width of ca. 81 G is in accord with couplings found for C3′• found in various systems,[21a,b,31] which have total widths (range 83−91 G). Thus, we assign this radical to the C3′•. We have simulated this C3′• spectrum by employing the following parameters (33 G (2βH), 15 G (1βH), 5 G Line-width) and the simulated spectrum matches with the major components of the spectrum in Figure 4D (see Supporting Information Figure S3). The hyperfine couplings used in this simulation of C3′• are very near to those found for the same radical in (i) a glassy (7 M LiCl/D_2O) solution of 5′-dGMP [35.2 G (2βH), 20.5 G (1βH), 7.6 G line-width][32] (ii) a single crystal of 5′-dGMP [16.7 G(1 βH), 27.5 G (1βH), and 38.2 G (1βH)].[31] Also, the spectrum in Figure 4D suggests the formation of UCH_2• in lower abundance.

A significant aspect of these experiments shown in Figure 4 and 1 is that the substitution of the azido (N_3) moiety at either the C5′- site (5′-AZT, Scheme 1) or at the C3′-site (3′-AZT, Scheme 1) results in reduced radical formation at that site by hydrogen abstraction. In 3′-AZT, the ESR spectrum in Figure 1E is dominated by UCH_2• (ca. 55%), and C5′• (ca. 35%). On the other hand, for 5′-AZT, as evident from Figure 4D, the predominant radical in the cohort is found to be C3′• (see Supporting Information Figure S3). These observed decreases in radical formation by substitution of the azido group at that site suggest bimolecular H-atom abstraction by aminyl radicals are governed by the C−H bond energies at the site of radical formation and are thus thermodynamically controlled.

B.1. Studies in D_2O versus H_2O. ESR spectral studies of electron attachment to 5′-AZT in homogeneous H_2O glasses (7.5 M LiCl/H_2O) were carried out as done for 5′-AZT samples in D_2O glasses (7.5 M LiCl/D_2O) and the results in H_2O glasses were compared with those found in D_2O glasses in Figure 5 below.

In Figure 5A, the first derivative ESR spectrum of the neutral aminyl radical (T(C5′)-ND•) (green color) shown in Figure 4B is presented. The spectrum of T(C5′)-ND• in Figure 5A has been simulated (blue color) and the simulated spectrum is superimposed on the experimentally observed spectrum (green) for comparison. We note here that a variety of conformations for T(C5′)-ND• exist (see Section 2.2), which give a variety of couplings for the two β-protons on the C5′ carbon. However the sum of the two β-proton couplings is relatively constant at 91 G (see Table 1) and this gives the appearance of the sharp

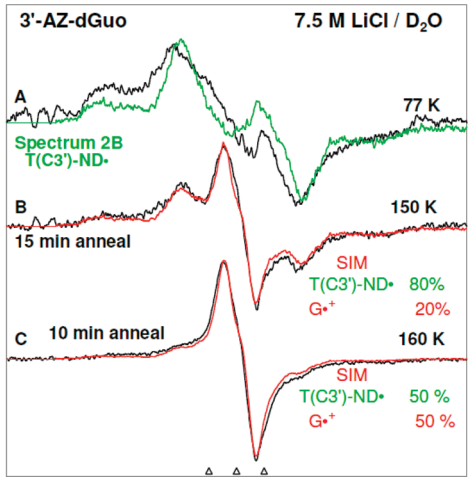

Figure 6. (A) ESR spectrum (black) recorded at 77 K after one-electron attachment in 3′-AZG at the native pD (ca. 5) in the homogeneous glassy solution of 7.5 M LiCl in D2O. $Cl_2^{\bullet-}$ has been subtracted from this spectrum. The spectrum (green) of T(C3′)-ND• (spectrum in Figure 1B) is superimposed on the experimentally recorded (black) spectrum for comparison. (B) ESR spectrum recorded at 77 K on annealing at 150 K for 15 min that allows for attack of $Cl_2^{\bullet-}$ on 3′-AZG producing one-electron oxidized guanine (G(-H)•). (C) Spectrum of one-electron oxidized G (black) and residual dG(C3′)-ND• recorded at 77 K after further annealing at 160 K for 10 min that allows for possible one-electron oxidation of G by dG(C3′)-ND•. The spectra (red) superimposed on the spectra (black) in (B) and (C) are simulations employing the spectra of T(C3′)-ND• (Figure 2B) and of $G^{\bullet+}$ [21a] as benchmark spectra.

outer peaks and the broadened inner two components. For details of the simulation, see Supporting Information S4.

In Figure 5B the first derivative ESR spectrum of the aminyl radical (T(C5′)-NH•) from 5′-AZT (red color) obtained under identical conditions to that in 5A except that it is in an H_2O glass. The total width of experimentally recorded spectrum of T(C5′)-NH• (red) is ca. 207 G. Comparison of the widths of experimentally recorded spectrum of T(C5′)-NH• (red) in B with that of T(C5′)-ND• (blue) clearly shows an additional coupling due to the α-H N−H (ca. 30 G). This additional proton hyperfine coupling is the $A_{||}$ (i.e., the A_{zz}) component of the proton coupling. This 30 G increase in the total width establishes that the source of the proton in the formation of the aminyl radical (T(C5′)-NH•), is the solvent (H_2O). We also mention here that a similar additional coupling due to the α-H N−H (ca. 28 G) was found for (T(C3′)-NH•) (see Figure 3).

Further annealing of this sample in the dark at 155 K for 30 min leads to the spectrum (red) recorded at 77 K (Figure 5C). For comparison, the ESR spectrum obtained via annealing of T(C5′)-N-D• at 170 K for 15 min in the dark in D_2O (7.5 M LiCl) (green color) from Figure 4D has been superimposed on it. The similarities of these two spectra establish that the radical cohort (UCH_2•, C3′•) formed in 5′-AZT due to bimolecular hydrogen abstraction by the aminyl radical (T(C5′)-NH•) in homogeneous H_2O glasses (7.5 M LiCl/H_2O) has very similar population of radicals to that for the corresponding reaction by the aminyl radical (T(C5′)-ND•) in homogeneous D_2O glasses suggesting no large solvent isotope effect.

C. Reactions Due to Electron Attachment in 3′-AZG. ESR spectral studies of electron attachment to 3′-AZG (see Scheme 1) were also carried out in homogeneous D_2O glasses (7.5 M LiCl/D_2O) and these results are presented in Figure 6 below.

The spectra shown in Figure 6A,B are those found after subtracting the $Cl_2^{\bullet-}$ and/or D• spectra. A small residual of the $Cl_2^{\bullet-}$ subtraction is found on the low field end of the spectrum. The original spectra before subtraction are shown in Supporting Information, Figure S5. Thus Figure 6A shows the first derivative ESR spectrum (black) recorded at 77 K in 3′-AZG after electron attachment. Superimposition of the authentic spectrum (green) of T(C3′)-ND• (spectrum in Figure 2B) on the black-colored spectrum in Figure 6A shows that the spectrum in Figure 6A predominantly consists of dG(C3′)-ND• and this radical has similar hyperfine couplings to T(C3′)-ND• (see Table 1).

Further annealing at 150 K for 15 min leads to the spectrum in Figure 6B (black) recorded at 77 K. The singlet at the center of this spectrum assigned to one electron oxidized guanine, results from one-electron oxidation of 3′-AZG by $Cl_2^{\bullet-}$ and dG(C3′)-ND•. Fom our previous work it is expected that $Cl_2^{\bullet-}$ would oxidize guanine.[18,21a,25] The oxidation by dG(C3′)-ND• is also expected from work with alkyl and aryl aminyl radicals act as one-electron oxidants (reaction 5) with the predicted midpoint potential at pH 7.0 of ca. 1.3−1.4 V.[33] A simulation (red) obtained by employing 80% of the (T(C3′)-ND•) spectrum shown in Figure 2B, and 20% of reported spectrum[21a] of one electron oxidized G, denoted as $G^{\bullet+}$ for simplicity as it is a mixture of the cation radical the deprotonated species. The simulation matches the experiment spectrum in Figure 6B quite well.

In Figure 6C, the spectrum (black) recorded at 77 K due to further annealing of this sample in the dark at 160 K for 10 min is shown. No observable line components due to sugar radicals are found in the spectrum shown in Figure 6C. A simulation (red) obtained by employing 50% of the (T(C3′)-ND•) spectrum and 50% of $G^{\bullet+}$ matches experiment quite well. This is consistent with additional one-electron oxidation of the guanine moiety in 3′-AZG by dG-(C3′)-ND• instead of abstraction from the sugar as was found with our 3′AZT results. However, the fact that $Cl_2^{\bullet-}$ was present at 150 K (Supporting Information Figure S5) complicates this analyses and a definitive answer awaits further work. While, one electron oxidation is the likely mechanism, we note that H-abstraction reactions from the guanine base[34] would not be distinguishable from one-electron oxidation followed by deprotonation.

2. Theoretical Studies. ***A. Initial Excess Electron Attachment Site.*** The molecular geometries of 3′-AZT and 5′-AZT were fully optimized in their neutral and the anion radical states. The lowest unoccupied molecular orbital (LUMO) of the neutral and singly occupied molecular orbital (SOMO) of the anion radical of 3′-AZT and 5′-AZT are shown in the Figure 7. From the orbital plot shown in Figure 7, it is evident that on anion radical formation, the excess electron is attached to the azido (N3) group of 3′-AZT or of 5′-AZT. For 3′-AZT, the electron affinity of the azido group is calculated to be ca. 0.31 eV, which is more than that of the thymine moiety. This theoretical conclusion is well-supported by the predominant formation ca. 80% of the neutral aminyl radical (T-(C3′)-ND•) from 3′-AZT via electron attachment at 77 K as found by the analysis of the ESR spectrum in Figure 2A.

B. HFCCs of the Neutral Aminyl Radical of 3′AZT (T(C3′)-NH•) and of 5′-AZT (T(C5′)-NH•). We have calculated the HFCC values from the optimized geometries of (T(C3′)-NH•) and of (T(C5′)-NH•); see Scheme 2. We find that there are small barriers to rotation in the aminyl radicals for rotation of the NH bond with respect to sugar moiety and they have a profound effect on the ESR spectra observed. In Scheme 2, we depict the rotation of the N1′−H′ bond around the C3′−N1′ bond in (T(C3′)-NH•). We carried out calculations of this rotation by a variation of the dihedral angle (H3′−C3′−N1′−H′) in 20° steps.

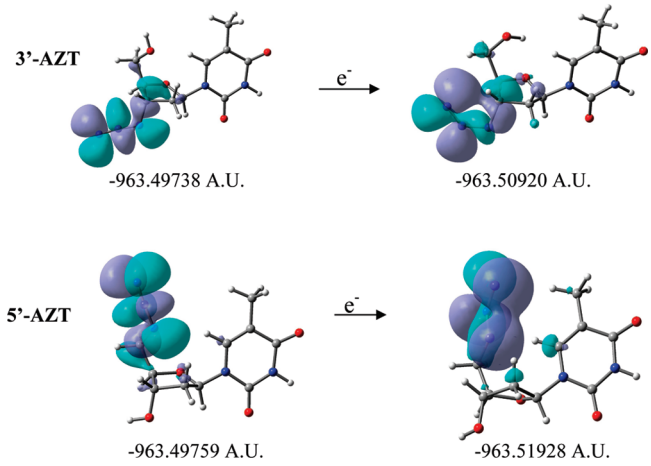

Figure 7. B3LYP/6-31G* optimized structures of 3′-AZT and 5′-AZT in the neutral state (showing the LUMO) and in the anion radical state (showing the SOMO) along with the total energies in atomic units. For 3-AZT, the anion radical is ca. 0.31 eV more stable than the neutral state showing a substantial gas phase EA of the azide group which is obviously greater than the thymine base.

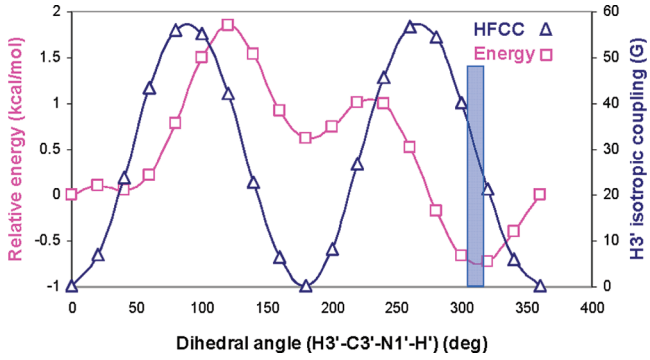

Figure 8. B3LYP/6-31G* calculated PES (pink) of (T(C3′)-NH•). The surface (pink) is calculated by rotating the N1′−H′ bond with respect to N1′−C3′−H3′ plane (i.e., the dihedral angle H3′−C3′−N1′−H′) in 20° steps. The variation of the DFT calculated HFCC values of H3′ with respect to the rotation of the dihedral angle H3′−C3′−N1′−H′ is also shown in blue color. The shaded area shows that very near (300°) DFT-calculated minimum energy, the calculated isotropic β-proton coupling of H3′ (40 G) matches its experimental (ca. 41 G, see Figure 2B).

Similarly, for (T(C5′)-NH•), the rotation of the N5′−H″ bond around the C5′−N5′ bond was modeled by 20° steps in the dihedral angle (H5″−C5′−N5′−H″). Using the DFT(B3LYP/6-31G*), we have scanned the potential energy surfaces (PES) by varying the dihedral angle (H3′−C3′−N1′−H′) in (T(C3′)-NH•) and the dihedral angle (H5″−C5′−N5′−H″) in (T(C5′)-NH•) as shown in Figures 8 and 9. The DFT-calculated β-proton isotropic hyperfine couplings are presented as well in each of the Figures 8 and 9 and are shown to vary as typical β-protons with dihedral angle.

Our calculations show that the N1′−H′ bond in T(C3′)-NH• is very flexible and involves ca. 2 kcal/mol energy for a complete 360° rotation of the dihedral angle (H3′−C3′−N1′−H′). The minimum of the PES lies between 300 and 320° (see Figure 8) and the theoretically calculated isotropic β-HFCC value of the H3′-atom of the C3′−H3′ bond in T(C3′)-NH• is found to be 40 G at 300° and 21 G at 320°. The value at 300° matches the experimental value (ca. 41 G) quite closely and is within 0.1 kcal of the bottom of the calculated PES. This conformational study suggests that the 300° conformation is the one that is experimentally found at 77 K (see Table 1).

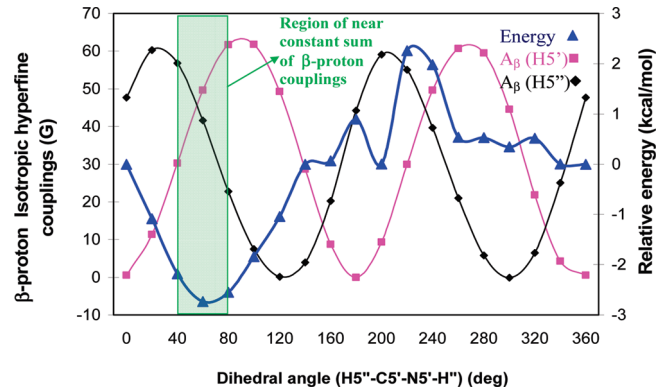

Figure 9. B3LYP/6-31G* calculated PES (blue color) for T(C5′)-NH•. The surface (blue color) is calculated by rotating the N5′−H″ bond with respect to N5′−C5′−H5″ plane (i.e., by rotating the H5″−C5′−N5′−H″ dihedral angle) in 20° steps. The variation of the DFT calculated HFCC values of H5′ (pink) and of H5″ (black) with the H5″−C5′−N5′−H″ dihedral angle is also shown. The shaded region from 40 to 80° shows a near constant sum of β-proton couplings (85−92 G), which matches the experimental sum (ca. 91 G, see Figure 4B) and corresponds to the minimum in energy ±0.5 kcal/mol.

The value of the A_{zz} component of anisotropic hyperfine coupling of the α-hydrogen atom attached to the N1′ in T(C3′)-NH• (see Scheme 2) is calculated to be −26.4 G (see Table 1), which matches well with the experimentally determined value of −28 G (Figure 3).

The calculated PES generated by rotation of the N5′−H″ bond around the N5′−C5′ bond in T(C5′)-NH• by varying the dihedral angle H5−N5′−C5′−H5 in 20° steps is shown in Figure 9. The global minimum is found to be at 60°. Changing the conformation by ±20° from the global minimum of 60° raises the energy by less than 0.5 kcal/mol, but the β-proton HFCC values of H5′ and H5″ vary significantly. Thus, at 60°, H5′ and H5″ have β-proton HFCCs of ca. 50 and 42 G, respectively. At 40°, the corresponding values of β-HFCCs for H5′ and H5″ are 30 and 57 G. However, at 80°, the corresponding values of β-HFCCs are ca. 62 and 23 G, respectively (see Table 1). Thus, the sum total of β-HFCCs of H5′ and H5″ in T(C5′)-NH• varies from 85 to 92 G and matches closely with the experimental total width of the doublet (the sum of these two β-HFCC values of ca. 91 G) shown in Figure 4B,C. Similar β-HFCCs of H5′ and H5″ were used ((50, 41) G, (30, 60) G, (70, 21) G to simulate (blue) the experimental spectrum (green) of (T(C5′)-ND•) shown in Figure 5A (see also Supporting Information S6).

In Table 1 below, we summarize our results for experimental hyperfine couplings and g-values of the neutral aminyl radical found in 3′-AZT and in 5′-AZT obtained from our analyses of the obtained spectra shown in Figures 2B and 3 (for 3′-AZT) and in Figures 4B and 5 (for 5′-AZT). The DFT calculated hyperfine couplings for these radicals are also presented and are found to match closely with the experimental values.

Conclusions

The experimental and theoretical studies reported in this work lead to the following salient conclusions:

1. The Azide moiety is the predominant site of electron attachment.

We find that the predominant site of electron capture in 3′-AZT and in its analogs is at the azide group. This experimental finding is supported by the theoretical calculations ((B3LYP/6-31G*, fully optimized) - which show that, in both 3′- and 5′-AZT, the gas phase electron affinity of the azide group is higher than that of the thymine moiety.

2. The neutral aminyl radical is found after one-electron attachment at 77 K.

At 77 K, the azide anion radical ($R-N_3^{\bullet-}$) produced via one-electron attachment on to the azide group in 3′-AZT, 5′-AZT, and 3′-AZG, spontaneously reacts to form the neutral aminyl radical (RNH•). The intermediates, $R-N_3^{\bullet-}$ and $RN^{\bullet-}$ expected from loss of N_2 are not observed. This shows that reactions 1 through 3 are complete even at 77 K for each of the azido compounds studied in this work.

3. H_2O is the source for protonation of the nitrene anion radical at 77 K

Our results in H_2O clearly show the spectral signature of the N−H α-proton hyperfine coupling (28 to 30 G) for the neutral aminyl radical that is lost in D_2O. The disappearance of this coupling in D_2O establishes that the source of the proton in the formation of the neutral aminyl radical is the solvent (H_2O).

Even under highly basic conditions (pD ca. 12, see Supporting Information Figure S4), only the neutral aminyl radical, R−NH•, is observed-which is in accord with the known high proton affinity of the parent nitrene radical ($R-N^{\bullet-}$).[8]

4. Conformational flexibility of the aminyl radicals.

Our DFT calculations show that rotation of the N−H group around the C3′−NH or C5′−NH bond in aminyl radicals have low barriers to rotation (ca. 3 kcal/mol for T(C3′)-NH•, and 5 kcal/mol for T(C5′)-NH•). This results in a range of conformations and corresponding β-proton couplings that have a range of values that broaden the ESR spectra.

5. Reactions of the neutral aminyl radicals, bimolecular H-atom abstraction and one-electron oxidation of guanine.

We find that abstraction reactions by the aminyl radicals are at the thymine methyl group and at the sugar sites at C5′ and C3′. The bond dissociation energy of the C−H bond in the methyl group of the thymine moiety is relatively low, ca. 86 kcal/mol (at 298 K),[35] whereas the sugar moiety sites are calculated to be higher.[36] The lower energy for abstraction from the methyl group in thymine forming UCH_2• explains why this radical is found to be the dominant species from the attack of T(C3′)-ND• on 3′-AZT. However, for T(C5′)-ND• attack on 5′-AZT, we find the predominant formation of C3′•, with a smaller extents of formation of C5′• and UCH_2•. We find decreases in radical formation at sites with substitution of the azido group. Thus for 5′-AZT the 3′ site and methyl group undergoes attack and for 3′-AZT the methyl group and 5′ site are attacked. This is consistent with an expected increase in C−H bond energies at a site with azide substitution.

For 3′-AZG samples, we find results that indicate the neutral aminyl radical 3′-dG-(C3′)-ND• is able to one-electron oxidize guanine. This finding suggests that sugar radicals produced by the attack of aminyl radicals on the sugar−phosphate backbone of DNA would be at the T and C sites since the lower redox potential of guanine and perhaps that of adenine would protect the sugar group attached to it from the H-atom abstraction.

Acknowledgment. This work was supported by the NIH NCI under Grant R01CA045424. Computational studies were supported by a computational facilities Grant NSF CHE-0722689. The authors acknowledge Dr. Anil Kumar for his help regarding theoretical calculations.

Supporting Information Available: S1: Simulation of the experimentally recorded ESR spectra of T(C3′)-ND• and T(C3′)-NH• shown in Figure 3 in the manuscript.

S2: Studies of electron attachment to 3′-AZT in D_2O at high pD (ca. 12).

S3: Radicals formed after γ-irradiation of a 7.5 M LiCl solution containing 5′-AZT (Figure S3A) at 77 K and subsequent annealing to higher temperatures (Figure S3B−D). Also, spectral evidence showing predominant formation of C3′• via intermolecular H-abstraction by T(C5′)-ND• in 5′-AZT.

S4: Simulation of the experimentally recorded ESR spectrum of T(C5′)-ND• shown in Figure 5A in the manuscript.

S5: Radicals formed after γ-irradiation of a 7.5 M LiCl solution containing 5′-AZG (Figure S5A) at 77 K followed by photoexcitation at 77 K and annealing to 150 K (Figure S5B,C).

Complete reference of ref 24 in the text. This material is available free of charge via the Internet at http://pubs.acs.org.

References and Notes

(1) Ta'rka'nyi, I.; Aradi, J. *Biochimie* **2008**, *90*, 156–172.
(2) Housri, N. ; Yarchoan, R.; Kaushal, A. *Cancer* **2010**, *116*, 273−283.
(3) Jagetia, G. C.; Aruna, R. *Toxicol. Lett.* **2003**, *139*, 33–43.
(4) Coucke, P. A.; Cottin, E.; Decosterd, L. A. *Acta Oncologica* **2007**, *46*, 612–620.
(5) Liao, Z.-K.; Zhou, F.-X.; Luo, Z.-G.; Zhang, W.-J.; Jie, X.; Bao, J.; Han, G.; Zhang, M.-S.; Xie, C.-H.; Zhou, Y.-F. *Oncol. Rep.* **2008**, *19*, 281–286.
(6) Zhou, F.-X.; Liao, Z.-K.; Dai, J.; Jie, X.; Xie, C.-H.; Luo, Z.-G.; Liu, S.-Q.; Zhou, Y.-F. *Biochem. Biophys. Res. Commun.* **2007**, *354*, 351–356.
(7) Westphal, E. M.; Blackstock, W.; Feng, W.; Israel, B.; Kenney, S. C. *Cancer Res.* **2000**, *60*, 5781–5788.
(8) McDonald, R. N.; Chowdhury, A. K.; Setser, D. W. *J. Am. Chem. Soc.* **1981**, *103*, 6599–6603.
(9) McDonald, R. N.; Chowdhury, A. K. *J. Am. Chem. Soc.* **1981**, *103*, 674–676.
(10) Zhou, Y.; Schuster, G. B. *J. Am. Chem. Soc.* **1990**, *112*, 8583–8585.
(11) Warrier, M.; Lo, M. K. F.; Monbouquette, H.; Garcia-Garibay, M. *Photochem. Photobiol. Sci.* **2004**, *3*, 859–863.
(12) Das, S.; von Sonntag, C. Z.; Naturforsch, B , *41B*, 505–513.
(13) von Sonntag, C. *Free-radical-induced DNA Damage and Its Repair*; Springer-Verlag: Berlin, 2006; pp 335−447.
(14) Mattson, D. M.; Ahmed, I. M.; Dayal, D.; Parsons, A. D.; Aykin-Burns, N.; Li, L.; Orcutt, K. P.; Spitz, D. R.; Dornfeld, K. J.; Simons, A. L. *Free Radical Biol. Med.* **2009**, *46*, 232–237.
(15) Messer, A; Carpenter, K.; Forzley, K; Buchanan, J; Yang, S.; Razskazovkii, Y.; Cai, Z.; Sevilla, M. D. *J. Phys. Chem. B* **2000**, *104*, 1128.
(16) Cai, Z.; Sevilla, M. D. *J. Phys. Chem. B.* **2000**, *104*, 6942.
(17) Cai, Z.; Sevilla, M. D. Long Range Charge Transfer in DNA II. In *Topics In Current Chemistry*; Schuster, G. B., Ed.; Springer-Verlag: Berlin, 2004; Vol. 237, p 103.
(18) Adhikary, A.; Khanduri, D.; Sevilla, M. D. *J. Am. Chem. Soc.* **2009**, *131*, 8614–8619.
(19) Adhikary, A.; Kumar, A.; Khanduri, D.; Sevilla, M. D. *J. Am. Chem. Soc.* **2008**, *130*, 10282–10292.
(20) Adhikary, A.; Kumar, A.; Munafo, S. A.; Khanduri, D.; Sevilla, M. D. *Phys. Chem. Chem. Phys.* **2010**, *12*, 5353–5368.
(21) (a) Adhikary, A.; Malkhasian, A. Y. S.; Collins, S.; Koppen, J.; Becker, D.; Sevilla, M. D. *Nucleic Acids Res.* **2005**, *33*, 5553–5564. (b) Adhikary, A.; Becker, D.; Collins, S.; Koppen, J.; Sevilla, M. D. *Nucleic Acids Res.* **2005**, *34*, 1501–1511. (c) Khanduri, D.; Collins, S.; Kumar, A.; Adhikary, A.; Sevilla, M. D. *J. Phys. Chem. B* **2008**, *112*, 2168–2178. (d) Adhikary, A.; Khanduri, D.; Kumar, A.; Sevilla, M. D. *J. Phys. Chem. B* **2008**, *112*, 15844–15855.
(22) (a) Becke, A. D. *J. Chem. Phys.* **1993**, *98*, 1372. (b) Stephens, P. J.; Devlin, F. J.; Frisch, M. J.; Chabalowski, C. F. *J. Phys. Chem.* **1994**, *98*, 11623.
(23) Lee, C.; Yang, W.; Parr, R. G. *Phys. Rev. B* **1988**, *37*, 785.
(24) Frisch, M. J.; et al. *Gaussian 03*, revision B.04; Gaussian, Inc.: Pittsburgh, PA, 2003 (for complete reference, see Supporting Information).
(25) Adhikary, A.; Kumar, A.; Becker, D.; Sevilla, M. D. *J. Phys. Chem. B* **2006**, *110*, 24170–24180.
(26) (a) Hermosilla, L.; Calle, P.; García, de la Vega, J. M.; Sieiro, C. *J. Phys. Chem. A* **2005**, *109*, 1114–1124. (b) Hermosilla, L.; Calle, P.; García, de la Vega, J. M.; Sieiro, C. *J. Phys. Chem. A* **2006**, *110*, 13600–13608.
(27) Close, D. M. *J. Phys. Chem. A* **2010**, *114*, 1860–1187.
(28) http://jmol.sourceforge.net. Jmol development team, An Open-Science Project, 2004 (accessed Jan 19, 2010).
(29) Shukla, L. I.; Adhikary, A.; Pazdro, R.; Becker, D.; Sevilla, M. D. *Nucleic Acids Res.* **2004**, *32*, 6565–6574.

(30) (a) Weiland, B.; Hüttermann, J. *Int. J. Radiat. Biol.* **1998**, *74*, 341–358, and references therein. (b) Weiland, B.; Hüttermann, J. *Int. J. Radiat. Biol.* **1999**, *75*, 1169–1175.

(31) Close, D. M. *Radiat. Res.* **1997**, *147*, 663–673.

(32) Shukla, L. I.; Pazdro, R.; Huang, J.; De Vreugd, C.; Becker, D.; Sevilla, M. D. *Radiat. Res.* **2004**, *161*, 582–590.

(33) Jonsson, M.; Wayner, D. D. M.; Lusztyk, J. *J. Phys. Chem.* **1996**, *100*, 17539–17543.

(34) (a) Steenken, S. *Chem. Rev.* **1989**, *89*, 503–520. (b) Candeias, L. P.; Steenken, S. *Chem.—Eur. J.* **2000**, *6*, 475. (c) Shinde, S. S.; Maroz, A.; Hay, M. P.; Anderson, R. F. *J. Am. Chem. Soc.* **2009**, *131*, 5203–5207.

(35) Li, X.; Sevilla, M. D.; Sanche, L. *J. Phys. Chem. B* **2004**, *108*, 19013–19019.

(36) Li, M.-J.; Liu, L.; Wei, K.; Fu, Y.; Guo, Q.-X. *J. Phys. Chem. B* **2006**, *110*, 13582–13589.

JP103403P